IEEE Access
Multidisciplinary | Rapid Review | Open Access Journal

Received February 15, 2020, accepted March 3, 2020, date of publication March 9, 2020, date of current version March 20, 2020.

Digital Object Identifier 10.1109/ACCESS.2020.2979186

Indoor Positioning Tightly Coupled Wi-Fi FTM Ranging and PDR Based on the Extended Kalman Filter for Smartphones

MENG SUN[1,2], YUNJIA WANG[1,2], SHENGLEI XU[2], HONGXIA QI[2], AND XIANXIAN HU[2]

[1]Key Laboratory of Land Environment and Disaster Monitoring, MNR, China University of Mining and Technology, Xuzhou 221116, China
[2]School of Environment Science and Spatial Informatics, China University of Mining and Technology, Xuzhou 221116, China

Corresponding author: Yunjia Wang (wyjc411@163.com)

This work was supported by the National Key Research and Development Program of China under Grant 2016YFB0502102.

ABSTRACT The smartphone-based Wi-Fi fine time measurement (FTM) technique has provided a new approach for Wi-Fi-based indoor location on mobile phones since the 2018 release of the Google Android Pie system, which supports the IEEE 802.11-2016 protocol and can directly measure the distance between the initiator and the responder. This paper studies in detail the properties of mobile phone Wi-Fi ranging and positioning performance. Considering non-line-of-sight (NLOS) error identification, a real-time ranging error compensation model based on the least-squares (LS) method and an adaptive Wi-Fi FTM positioning algorithm (AWFP) utilizing the weighted least-squares (WLS) method are devised. To improve accuracy, a new tightly coupled fusion positioning algorithm integrating Wi-Fi FTM and built-in mobile phone sensors based on the extended Kalman filter (EKF) is constructed. The experimental results show that the ranging precision and Wi-Fi positioning accuracy are improved. Based on the high-precision Wi-Fi ranging and positioning results, the final location accuracy of the proposed fusion method is 0.98 m, and the root-mean-square error (RMSE) is 1.10 m, which are better than those of the PDR, Wi-Fi FTM and loosely coupled PDR/Wi-Fi FTM integration based on the EKF.

INDEX TERMS Indoor positioning, Wi-Fi FTM, pedestrian dead reckoning, tightly coupled, ekf.

I. INTRODUCTION

Indoor positioning is attracting increasing attention because of the rapid development of society and the increased demand for location-based services (LBSs) in people's lives [1], [2]. The Global Navigation Satellite System [3] (GNSS) cannot work well in indoor environments because it suffers from serious multipath propagation problems caused by complex indoor topologies, electronic facilities, and many other factors. Therefore, many types of wireless signals such as Wi-Fi [4]–[6], Bluetooth [7], RFID [8], [9], Zigbee [10], UWB [11], and magnetic fields [12] have been studied to solve indoor positioning problems and model the mobility of urban crowds in modern smart-cities [13]. Different approaches have different advantages and shortcomings. Although geomagnetic positioning can reach high positioning precision with certain algorithms [14], it is difficult for researchers to use it effectively due to factors like electronic facilities and magnetic field changes. There are currently no technologies that can balance positioning accuracy and costs [2]. Micro-Electro-Mechanical Systems (MEMSs) provide multiple and powerful sensors for indoor positioning. Pedestrian dead reckoning (PDR) [15]–[17] is a kind of technology that can estimate positions by using a gyroscope, magnetometer and accelerometer. This method can temporarily output relative positions, but the system error caused by azimuth estimation, step detection and other factors accumulates over time [17], which results in large errors. Therefore, integrating PDR with other techniques is usually applied to restrict the error accumulation.

Among these numerous indoor positioning technologies, the Wi-Fi positioning technique is a widely studied method by researchers due to its convenient application in most buildings and the WLAN connectivity of mobile phones. Traditionally, Wi-Fi positioning has been divided into different strategies based on different positioning theories, such as using

The associate editor coordinating the review of this manuscript and approving it for publication was Anton Kos.

the received signal strength indicator (RSSI) [18], time of arrival (TOA) [19], time of difference arrival (TDOA) [20] and channel state information (CSI) [21]. RSSI-based Wi-Fi positioning needs a high-precision fingerprint database to achieve high positioning accuracy, and it is easier to implement on smartphones. However, the heavy efforts required to update and construct the database restrict its application in large-scale buildings. Time-based methods including the TOA and TDOA need time synchronization to get high-precision time measurements [22], which is critical for high ranging and positioning accuracy. However, it is difficult to realize strict time synchronization. A CSI-based technique can reach meter-level precision, but it requires special hardware support and is also difficult to implement. Apart from the above approaches, another time-based Wi-Fi positioning method using the improved time of flight [23] (TOF) protocol is receiving increasing attention due to its high positioning accuracy. This TOF protocol can provide precise time measurements and is also the basis of the fine time measurement (FTM) technique, which has been introduced and standardized by the IEEE 802.11 working group [24]. It can compensate for the lack of time synchronization by measuring the round-trip-time (RTT). The distance between the initiator and responder can be calculated by multiplying the RTT and the speed of light, which greatly reduces the difficulty of realizing time-based Wi-Fi positioning.

The integration of different technologies, such as PDR integrating geomagnetic positioning [25], and combining Wi-Fi with geomagnetic and PDR [26] is becoming very popular. Filtering algorithms like the Kalman filter (KF) [27]–[29], the extended Kalman filter (EKF) [11], [26], and the particle filter (PF) [25], [30] have been employed. Generally, combining the results of different methods by utilizing filtering algorithms, as in [28] and [29], is defined as loosely coupled fusion. On the other hand, directly using the observation measurements for integration, as in [8] and [11], is defined as tightly coupled fusion. Considering nonlinear motions and scenarios, the EKF and tightly coupled fusion methods are more suitable for actual applications. Although the PF also has good performance in solving nonlinear problems, the high computational load and particle degradation problem restrict its application on mobile terminals [14]. In our research, the EKF algorithm was selected to combine PDR with the improved Wi-Fi FTM positioning method. A tightly coupled model was constructed based on the EKF. In the Wi-Fi positioning module, we devised different strategies to solve problems including the ranging error compensation and the limitation of trilateration algorithm. Our contributions are as follows:

1) We analysed the properties of Wi-Fi FTM ranging by using mobile phones in different circumstances and proposed the real-time ranging model that considers the error compensation and the identified NLOS error. Less than one-meter ranging accuracy could be obtained;

2) We devised an adaptive Wi-Fi positioning algorithm based on the weighted least-squares (WLS) method. This algorithm could dynamically adjust the ranging data to meet the positioning conditions and the final location accuracy was better than that of the traditional Wi-Fi trilateral positioning method;

3) We proposed the Wi-Fi FTM and PDR tightly coupled fusion positioning model based on the EKF algorithm and validated positioning performance in a typical office environment. The experimental results demonstrate that the proposed method has better performance regarding its positioning accuracy and stability.

The remainder of this paper is organized as follows: Section II is about the related works of Wi-Fi FTM; Section III describes the PDR method, Wi-Fi FTM and the tightly coupled fusion positioning algorithm; the experimental setup and results are stated in Section IV; Section V draws the conclusion and future works.

II. RELATED WORKS

Time-based Wi-Fi positioning techniques using TDOA protocol [20], [22] and TOA protocol [19], [31] have been studied by many researchers and these related works show that this technology is very attractive, even if it is difficult to implement on mobile phones and requires special hardware support. In 2013, Banin *et al.* [23] studied in detail how the Wi-Fi TOF protocol works and conducted ranging and positioning experiments in an office environment. Then, in 2016, the new release of the IEEE 802.11 wireless local area network (WLAN) standard [24] allowed for measurement of the distance of two Wi-Fi stations by utilizing the Wi-Fi fine time measurement (FTM) technology, which is based on the TOF protocol. Therefore, in order to develop the Wi-Fi FTM protocol in a highly non-linear indoor environment, Banin *et al.* [32] compared the performances of the Kalman filter (KF) and Bayesian filter (BF) and confirmed that the BF performed better than the KF. They combined Wi-Fi FTM positioning with map information by using the BF and achieved accurate experimental results. Moreover, the ranging estimation model based on the artificial neural network (ANN) was also presented in [33], the ANN was trained in a supervised-learning manner and implemented by using the Google TensorFlow framework API. Experiments showed that Wi-Fi FTM ranging estimation using the ANN model could outperform the maximum likelihood estimation (MLE) [34]. Ibrahim *et al.* [35] introduced an open platform for experimenting with FTM and analysed the factors and parameters that can influence the ranging performance. They noted that meter-level ranging accuracy can be reached after correcting ranging errors in low-multipath environments. All of these studies provide a solid foundation for Wi-Fi FTM ranging positioning and make it highly researchable.

In 2018, Google Developer Days (GDD) introduced the new Android Pie system [36], which enables mobile phones to measure the round-trip-time (RTT) with respect to other Wi-Fi access points by using the Wi-Fi FTM protocol. This is a revolutionary update because developers can measure the distances between themselves and Wi-Fi stations by

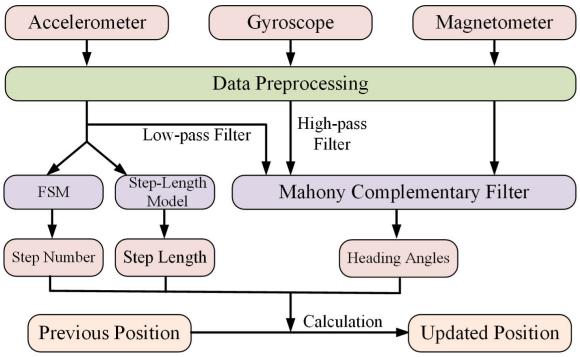

FIGURE 1. The framework of the PDR method in this work.

multiplying the RTT and the speed of light, which means that indoor positioning can be realized by using Wi-Fi FTM on smartphones. Therefore, related scientific researches begin to increase. Yue *et al.* [37] presented a real-time Wi-Fi ranging model that can effectively eliminate the ranging errors caused by clock deviations, non-line-of-sight (NLOS) and multipath propagation. The unscented Kalman filter (UKF) was finally utilized to fuse the robust dead reckoning and Wi-Fi FTM. Their experimental results showed that the mean positioning errors were within 2 m. Xu *et al.* [38] provided two different strategies to update the particle set in the enhanced particle filter and employed it to combine the PDR and Wi-Fi FTM. The experimental results indicated that the mean positioning accuracy was approximately 1 m, and the new position was given within 0.5 second. In addition, the problem regarding how to simultaneously track thousands of Wi-Fi users was studied in [39]. The collaborative time of arrival (CTOA) protocol was designed, which relies on the periodic broadcasts transmitted by the broadcasting stations (bSTA). A positioning accuracy of roughly 2 m in 95% of the cases was reached in congested and multipath-dense environments.

Overall, the related research on Wi-Fi FTM ranging is still in its infancy. Compared with other indoor positioning techniques, Wi-Fi FTM ranging positioning has a promising future and high application value due to its convenience and high positioning accuracy.

III. THEORIES AND METHODS

A. PEDESTRIAN DEAD RECKONING

Pedestrian dead reckoning (PDR) is a relative positioning method that mainly includes three parts: heading angles estimation, step detection and step length estimation. The general process of PDR is illustrated in Fig.1. If the initial position is known, the updated position can be calculated by using (1):

$$\begin{bmatrix} N_{k+1} \\ E_{k+1} \\ l_{k+1} \end{bmatrix} = \begin{bmatrix} 1 & 0 & \cos\psi_k \\ 0 & 1 & \sin\psi_k \\ 0 & 0 & 1 \end{bmatrix} \begin{bmatrix} N_k \\ E_k \\ l_k \end{bmatrix} + \begin{bmatrix} \sigma_1 \\ \sigma_2 \\ \Delta l \end{bmatrix} \quad (1)$$

where N_k and E_k represent the coordinate values of the carrier at the north and east direction at time k, respectively; l_k and ψ_k represent the step length and heading angle at time k, respectively; σ_1 and σ_2 are the system errors; and Δl is the change of the step length. If $\boldsymbol{X}(k)$ represents the position at time k, (1) can be expressed as:

$$\boldsymbol{X}_{k+1} = \Phi \cdot \boldsymbol{X}_k + \boldsymbol{G}_k \quad (2)$$

1) HEADING ANGLES ESTIMATION

Generally, the heading angles can be measured by using a gyroscope [40], a magnetometer, an accelerometer [41], [42], and the fusion of different sensors [43]. Different algorithms have different shortcomings, such as the integration problems when using a gyroscope and the sensitivity of magnetometer to the environment. To make full use of different types of sensor data, the Mahony complementary filter (MCF) [44] is adopted in our research to estimate the heading angles. This algorithm mainly utilizes the gyroscope data to calculate the heading angles, but the accelerometer and magnetometer will correct the gyroscope in time so that the estimation errors will not accumulate. The whole producer contains two parts, which are the error compensation calculation and the gyroscope data correction. First, the gyroscope data is expressed as the quaternion vector to represent the current attitude prediction. The quaternion vector is represented as:

$$\boldsymbol{Q} = \begin{bmatrix} q_0 & q_1 & q_2 & q_3 \end{bmatrix}^T \quad (3)$$

Assuming the gyroscope error compensation is $\boldsymbol{e}$, it can be defined as follows:

$$\boldsymbol{e} = \boldsymbol{e}_a + \boldsymbol{e}_m \quad (4)$$

where $\boldsymbol{e}_a$ and $\boldsymbol{e}_m$ are the error correction items calculated by using the accelerometer and magnetometer data, respectively, and their equations are as follows:

$$\begin{cases} \boldsymbol{e}_a = (\boldsymbol{C}_n^b \cdot \boldsymbol{g}_a) \times \boldsymbol{a} \\ \boldsymbol{e}_m = (\boldsymbol{C}_n^b \cdot \boldsymbol{b}_m) \times \boldsymbol{m} \end{cases} \quad (5)$$

where $\boldsymbol{g}_a$ is the gravity vector in the geographic coordinate system, where $\boldsymbol{g}_a = \begin{bmatrix} 0 & 0 & g \end{bmatrix}^T$, and $g = 9.8m/s^2$; $\boldsymbol{b}_m$ is the geomagnetic vector when the x-axis of device points to the north, where $\boldsymbol{b}_m = \begin{bmatrix} b_{mx} & 0 & b_{mz} \end{bmatrix}^T$; $\boldsymbol{a}$ and $\boldsymbol{m}$ are the normalized measured accelerometer and magnetometer data; $\boldsymbol{C}_n^b$ is the rotation matrix from the geographic coordinate system to the carrier coordinate system; and "$\times$" represents the vector cross product, respectively. After obtaining these two error corrections, the corrected gyroscope data is defined as:

$$\boldsymbol{\omega} = \boldsymbol{\omega}_g + K_P \boldsymbol{e} + K_I \int \boldsymbol{e} \quad (6)$$

where $\boldsymbol{\omega}_g = \begin{bmatrix} \omega_{gx} & \omega_{gy} & \omega_{gz} \end{bmatrix}^T$ and $\boldsymbol{\omega} = \begin{bmatrix} \omega_x & \omega_y & \omega_z \end{bmatrix}^T$ are the normalized gyroscope raw data and the corrected gyroscope data, respectively; K_P and K_I are the error control items, which are 2.0 and 0.001 in our research work, respectively. Then, the corrected gyroscope data should be substituted into the quaternion differential equation and the first-order

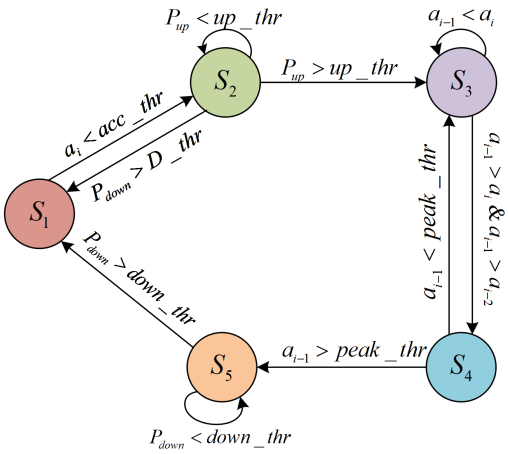

FIGURE 2. Execution process of the FSM algorithm.

Runge-Kutta method [45] is used to get the quaternion update equation as follows:

$$\begin{cases} q_0(t+T) = q_0(t) - \dfrac{T}{2}\left[\omega_x q_1(t) + \omega_y q_2(t) + \omega_z q_3(t)\right] \\ q_1(t+T) = q_1(t) + \dfrac{T}{2}\left[\omega_x q_0(t) + \omega_z q_2(t) - \omega_y q_3(t)\right] \\ q_2(t+T) = q_2(t) + \dfrac{T}{2}\left[\omega_y q_0(t) - \omega_z q_1(t) + \omega_x q_3(t)\right] \\ q_3(t+T) = q_3(t) + \dfrac{T}{2}\left[\omega_z q_0(t) + \omega_y q_1(t) - \omega_z q_2(t)\right] \end{cases} \tag{7}$$

where $q_i(t)$ and $q_i(t+T)$ are the quaternion values at time t and $(t+T)$, respectively, and $i = 1, 2, 3, \cdots$; T is the sampling time interval. The updated quaternion values should be normalized and substituted into (8) to obtain the azimuth:

$$\psi = \mathrm{tg}^{-1}\frac{2(q_1 q_2 + q_0 q_3)}{1 - 2(q_2^2 + q_3^2)}, \quad \psi \in (0, 2\pi) \tag{8}$$

Moreover, it should be pointed out that the low-pass filter [46] and the high-pass filter [47] are applied to process the observation noise in the acceleration and gyroscope raw data, respectively. Due to the high sampling rate of mobile phone sensors, several heading angles will be output. Therefore, a mean filter algorithm [48] is used to filter out the outliers, and the mean heading angle in one second is the final heading estimation result. In our experiments, the MCF algorithm can provide a mean estimation accuracy of the azimuth that is better than 10°.

2) STEP DETECTION AND STEP-LENGTH ESTIMATION

Many step detection algorithms have been proposed by researchers, such as the peak detection method [49] and the zero velocity update method [50]. As shown in Fig.2, acceleration values regularly change when a human is walking. The peak detection method can utilize the acceleration peaks and valleys to detect steps. It is easier to implement than other methods. However, the measurement errors and false peaks affect the recognition accuracy. Therefore, we employ the finite-state machine (FSM) in the step detection process because it is also easy to implement and more resistant to interference from errors.

TABLE 1. Variable names and values.

Variables	Description of Variables	Value
acc_diff	Acceleration difference threshold	0.05
acc_thr	Entering algorithm threshold	9.8
up_thr	Maximum value judged as rising state	5.0
down_thr	Minimum value judged as rising state	5.0
peak_thr	Peak threshold	10.8
D_thr	Max interference value	4.0

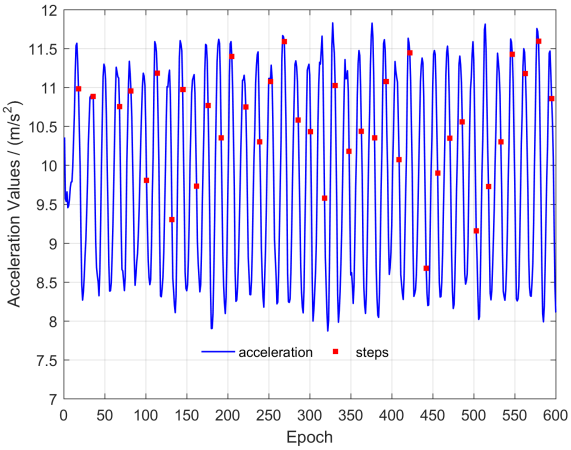

FIGURE 3. Acceleration of the walking process for 38 steps.

Fig.2 shows the whole producer of the FSM algorithm. It divides the walking process into five states $S_1 \sim S_5$. S_1 is the static state and the acceleration value is approximately 9.8 m/s^2; S_2 is the taking steps state, and the acceleration gradually increases; S_3 is the finding peaks state, and S_4 is the peak threshold judgement; S_5 represents the falling state and the acceleration decreases. If these five states satisfy the threshold conditions, one step is recognized. During the execution process, FSM also introduces the noise shielding mechanism, which can effectively eliminate the influence of measurement noise. Two state values P_{up} and P_{down} are defined and their values are updated by using the following:

$$\begin{cases} P_{up} = P_{up} + 1, & a_i - a_{i-1} > acc\_diff \\ P_{down} = P_{down} + 1, & a_i - a_{i-1} < acc\_diff \end{cases} \tag{9}$$

where a_i and a_{i-1} are the acceleration values at time i and $i-1$, respectively. If large measurement noise exists, P_{up} and P_{down} increase by one. The walking state will return to S_1 if P_{down} is larger than the max interference value D_thr. In the meantime, P_{up} and P_{down} are reset to zero. The variable names and values, and the detection results for 38 steps are shown in Table 1 and Fig.3, respectively.

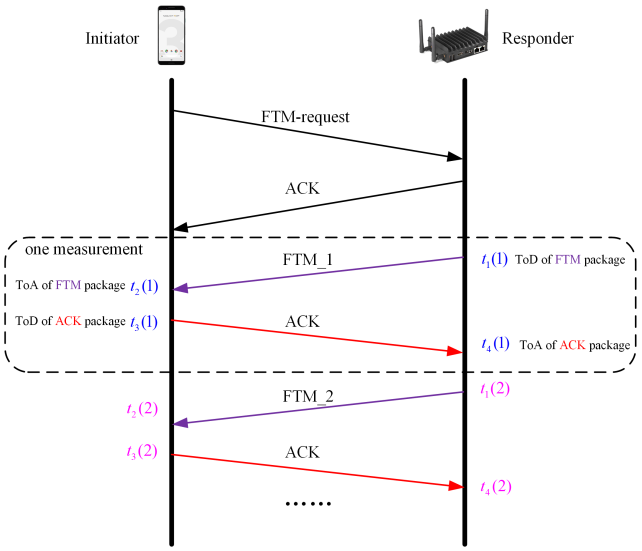

FIGURE 4. The producer of the Wi-Fi FTM.

Studies have shown that the step length of people walking is related to the acceleration. Apart from the acceleration, the step length also differs due to the heights and strides of different people. The existing step length estimation models include linear models [38], [51], constant models [52] and nonlinear models [17], [53], but there is currently no universal step length estimation model. Different algorithms have similar performances. In our research, the Weinberg model [54] is employed to calculate the step length and it can be calculated as follows:

$$SL = K \cdot \sqrt[4]{a_{max} - a_{min}} \tag{10}$$

where K is the scale factor of the step length, a_{max} and a_{min} are the maximum and minimum acceleration in one step period, respectively.

B. WIFI FTM RANGING POSITIONING USING SMARTPHONES

1) THEORETICAL RANGING MODEL BASED ON THE WIFI FINE TIME MEASUREMENT

Wi-Fi FTM protocol enables smartphones (initiator stations, ISTA) to simultaneously measure the distances from different Wi-Fi APs (responder stations, RSTA) if these APs support the IEEE 802.11-2016 protocol. As shown in Fig.4, the whole FTM producer is as follows. First, the ISTA sends an FTM request to the RSTA and wait for its ACK message. Second, the RSTA receives the FTM request and sends the ACK message back to the ISTA. Then, several FTM feedbacks are sent to the ISTA from the RSTA and the ToD (time-of-departure) $t_1(1)$ of the FTM package is recorded by the RSTA. The ToA (time-of-arrival) $t_2(1)$ of the FTM package will also be measured once the ISTA receives it. A similar process of the ACK package exchange is performed and the ToD $t_3(1)$ and ToA $t_4(1)$ are recorded. Then, one FTM exchange has been completed and the mean round-trip time (RTT) can be

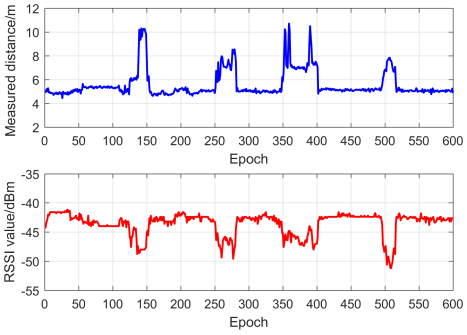

FIGURE 5. RSSI and ranging data containing NLOS error.

estimated if there are n FTM-ACK exchanges by using (11):

$$RTT = \frac{1}{n} \cdot \sum_{k=1}^{n} ([t_4(k) - t_1(k)] - [t_3(k) - t_2(k)]) \tag{11}$$

After obtaining the mean round-trip-time, the distance between the ISTA and RSTA can be obtained by multiplying the RTT and the speed of light C. The theoretical ranging model can be defined as follows:

$$D_{RTT} = \frac{C}{2n} \cdot \sum_{k=1}^{n} ([t_4(k) - t_1(k)] - [t_3(k) - t_2(k)]) \tag{12}$$

However, there are many factors that can affect the Wi-Fi ranging process, such as the time delay of hardware, non-light-of-sight (NLOS) error and multipath propagation [37]. Taking all these errors items into account, the traditional ranging model is expressed as follows:

$$Dist = \frac{C}{2n} \cdot \sum_{k=1}^{n} ([t_4(k) - t_1(k)] - [t_3(k) - t_2(k)]) - D_{delay} - D_{NLOS} - D_m + \varepsilon \tag{13}$$

where D_{delay}, D_m and D_{NLOS} are the ranging errors caused by the time delay of hardware, multipath propagation and the NLOS, respectively; ε is the random error. Even though different factors cause different ranging errors, all these factors contribute to the total ranging errors. However, D_{NLOS} is special, and it always appears when the responders or smartphones are blocked by human bodies, buildings and other factors. This kind of error does not exist all the time and it is difficult to eliminate. Conversely, D_{delay} and D_m, which are caused by the hardware and the environmental factors respectively, always exist in the ranging data. Therefore, it is necessary for us to identify the appearance of NLOS error and compensate for other ranging errors.

2) NLOS ERROR IDENTIFICATION AND REAL-TIME RANGING ERROR COMPENSATION BASED ON THE LEAST SQUARES METHOD

In addition to the measured distance, the received signal strength indicator (RSSI) of different RSTAs can also be measured in the ranging process. As shown in Fig.5, both of

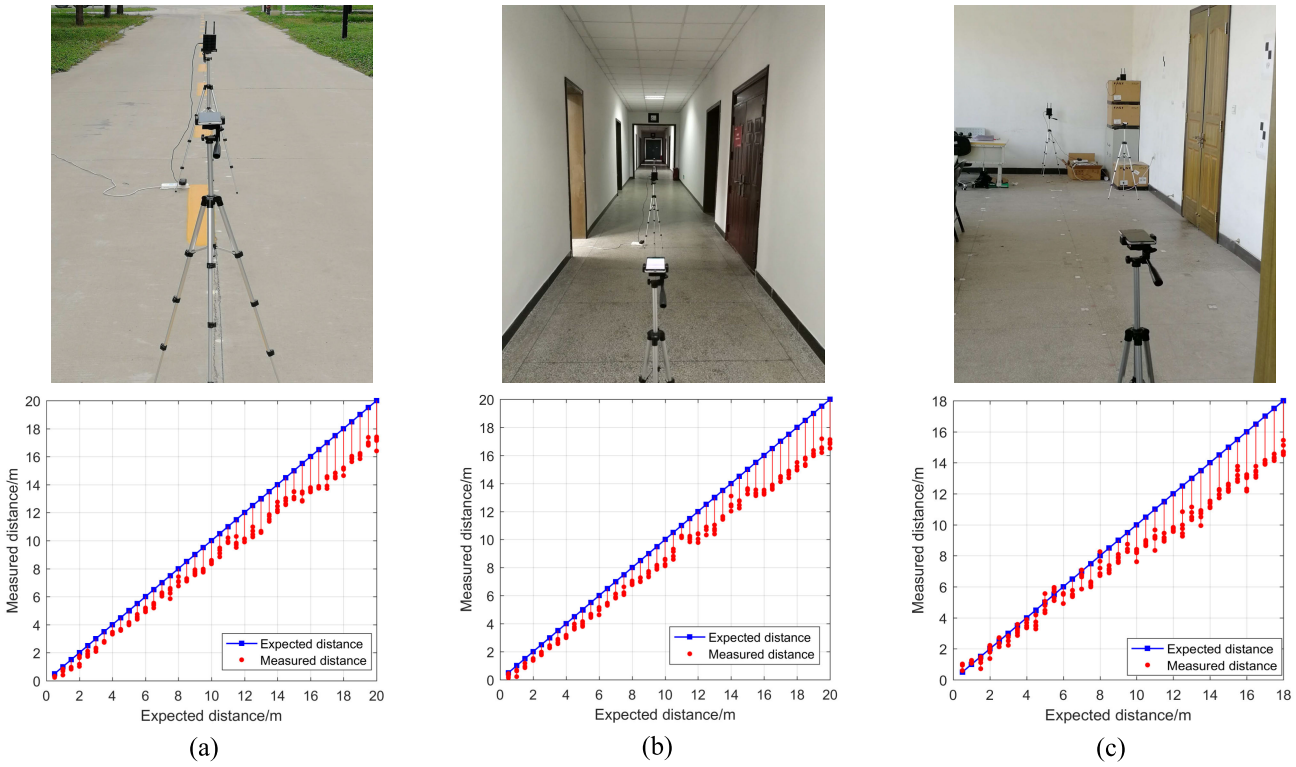

FIGURE 6. Measured distances VS expected distances in different circumstances. (a) Outdoor, (b) Corridor, and (c) Indoor room.

them will generate large fluctuations if the device is blocked, which means that the fluctuations of the RSSI and distance data can reflect the appearance of NLOS errors.

Therefore, the standard deviations of the RSSI and ranging data in one second are utilized to detect the NLOS errors and the identification condition can be defined as follows:

$$S = S_r \cup S_d \tag{14}$$

where S is the identification result and the NLOS error is detected when its value is 1, $\cup$ is the union of S_d and S_r, which are the detection results from using the standard deviations of the measured ranging data and the RSSI data from each responder in one second, respectively. S_d and S_r are set to 1 if they meet the threshold conditions, which can be obtained by training a large amount of data. In our research work, the ranging data of one responder is abandoned if it contains NLOS error. Therefore, it is not included in the positioning calculations. If there is no NLOS error detected, the other ranging errors should be compensated by using the following compensation model.

Fig.6 shows the differences of the measured ranging data and the expected ranges in different circumstances. It is clear that the differences between them increase as the device becomes further away from the responder, which means that the ranging error varies nonlinearly with the distance. This is consistent with the experimental result in [32]. Thus, the discrete points fitting method based on the least-squares (LS) method is adopted to fit the ranging errors and the distance data. Once the fitting coefficients are obtained, the error compensation and the accurate ranging data can be calculated. We assume that the ranging error and the expected range satisfy the following relationship:

$$e_i = a_0 + a_1 d_i + a_2 d_i^2 + \ldots + a_m d_i^m \tag{15}$$

where a_i is the coefficient, e_i is the ranging error and d_i is the actual distance. If there are n ranging errors data, the equation can be expressed as follows:

$$\begin{cases} e_1 = a_0 + a_1 d_1 + a_2 d_1^2 + \ldots + a_m d_1^m \\ e_2 = a_0 + a_1 d_2 + a_2 d_2^2 + \ldots + a_m d_2^m \\ \vdots \\ e_n = a_0 + a_1 d_m + a_2 d_m^2 + \ldots + a_m d_m^m \end{cases} \tag{16}$$

Equation (16) can also be expressed in the following formula:

$$\begin{bmatrix} e_1 \\ e_2 \\ \vdots \\ e_n \end{bmatrix} = \begin{bmatrix} 1 & d_1 & \cdots & d_1^m \\ 1 & d_2 & \cdots & d_2^m \\ \vdots & \vdots & \cdots & \vdots \\ 1 & d_m & \cdots & d_m^m \end{bmatrix} \cdot \begin{bmatrix} a_0 \\ a_1 \\ \vdots \\ a_m \end{bmatrix} \tag{17}$$

If (17) meets the condition: $n > (m+1)$, the coefficients can be calculated by using the LS method:

$$\boldsymbol{A} = (\boldsymbol{D}^T \boldsymbol{D})^{-1} \boldsymbol{D}^T \boldsymbol{E} \tag{18}$$

where $\boldsymbol{A}$, $\boldsymbol{D}$ and $\boldsymbol{E}$ are the fitting coefficients matrix, the error matrix and the distance matrix in equation (17), respectively.

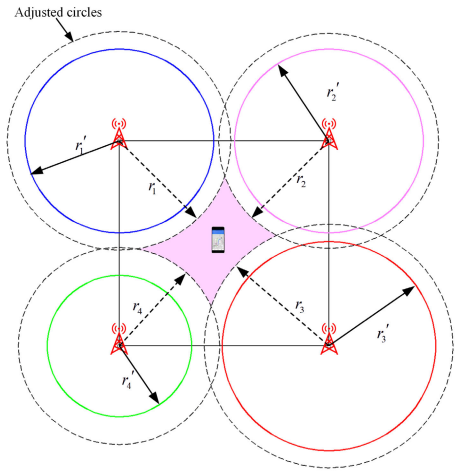

FIGURE 7. Disjoint circles and radius adjustment.

After obtaining the coefficients, the error compensation item can be computed. The real-time ranging model considering the NLOS error identification and error compensation is defined as follows:

$$Dist = D_{RTT} - (a_0 + a_1 D_{RTT} + \ldots + a_m D_{RTT}^m) + \varepsilon, S = 1 \tag{19}$$

3) ADAPTIVE WIFI FTM POSITIONING ALGORITHM BASED ON THE WEIGHTED LEAST-SQUARES METHOD

After getting the compensated distances, the positions can be calculated by using the trilateral positioning algorithm [55] if there are three or more responders detected. Due to the measurement errors, these circles with the radiuses of the compensated ranging data will not intersect at one point. Furthermore, as shown in Fig.7, these circles do not intersect at all. In this condition, the trilateral positioning algorithm would not work well. Therefore, an adaptive Wi-Fi FTM positioning algorithm (AWFP) based on the weighted least squares-method (WLS) is proposed. This algorithm mainly contains intersection detection and radius adjustment. The intersection detection judges whether these circles intersect. If $ins = 1$ represents the intersection of two circles, the basic judging condition can be defined as follows:

$$ins = 1, (r_1 - r_2) < cd < (r_1 + r_2) \tag{20}$$

where r_1 and r_2 are the radiuses, which are also the compensated ranging data; and cd is the center distance, which is the distance of two APs. If these circles do not intersect, their radiuses should be adjusted until they intersect with one another. The radius adjustment rule is defined as:

$$r_i = r_i + \sum_{j=1}^{j} \frac{1}{r_i} \tag{21}$$

where j is the number of times that the radius is adjusted. The radius adjustment process is shown in Fig.7. Every time that the radius is adjusted, the algorithm will judge whether the circles intersect. Once all the circles interest, the WLS method is adopted to calculate the positions. Generally, the measured distance is smaller if the tester is closer to one responder. Therefore, we should give greater weight to the ranging data of the closest responder because it is more reliable. The weight of each circle can be calculated by using (22):

$$\omega_i = r_i^{-q} \Big/ \sum_{i=1}^{n} r_i^{-q} \tag{22}$$

where r_i is the adjusted ranging data, $i = 1, 2, \cdots, n$; and q is a positive integer with a value of 1. Then, the real-time 2D position is calculated by using (23):

$$\boldsymbol{U} = (\boldsymbol{B}^T \boldsymbol{P} \boldsymbol{B})^{-1} \boldsymbol{B}^T \boldsymbol{P} \boldsymbol{L} \tag{23}$$

where $\boldsymbol{U}$ is the Wi-Fi position estimation,

$$\boldsymbol{U} = (x, y)\boldsymbol{B} = \begin{bmatrix} 2x_{RTT}^1 - 2x_{RTT}^2 & 2y_{RTT}^1 - 2y_{RTT}^2 \\ 2x_{RTT}^1 - 2x_{RTT}^3 & 2y_{RTT}^1 - 2y_{RTT}^3 \\ \vdots & \\ 2x_{RTT}^1 - 2x_{RTT}^n & 2y_{RTT}^1 - 2y_{RTT}^n \end{bmatrix},$$

$$\boldsymbol{P} = \begin{bmatrix} |\omega_2 - \omega_1| & 0 & \cdots & 0 \\ 0 & |\omega_3 - \omega_1| & \cdots & 0 \\ \vdots & \vdots & \ddots & \vdots \\ 0 & 0 & \cdots & |\omega_n - \omega_1| \end{bmatrix},$$

$$\boldsymbol{L} = \begin{bmatrix} r_2^2 - r_1^2 - x_{RTT}^{22} - y_{RTT}^{22} + x_{RTT}^{12} + y_{RTT}^{12} \\ r_3^2 - r_1^2 - x_{RTT}^{32} - y_{RTT}^{32} + x_{RTT}^{12} + y_{RTT}^{12} \\ \vdots \\ r_n^2 - r_1^2 - x_{RTT}^{n2} - y_{RTT}^{n2} + x_{RTT}^{12} + y_{RTT}^{12} \end{bmatrix},$$

n is the number of APs, and x_{RTT}^n and y_{RTT}^n are the coordinates values of $n - th$ responder. The producer of AWFP is shown in algorithm 1.

C. TIGHTLY COUPLED FUSION POSITIONING MODULE

1) FUSION SYSTEM VARIABLE DEFINITIONS

Since the EKF and tightly coupled methods are suitable for the nonlinear applications, inspired by the research in [8] and [11], we constructed a new PDR/Wi-Fi FTM tightly coupled model. Because the distances between system's current position and responders could be calculated and the ranging data from responders can also be obtained, we utilize these distances to construct the systematic observation. First, the PDR position is utilized as the system state. Considering the Wi-Fi positions, the system equation is defined as follows:

$$\boldsymbol{X}(k) = \boldsymbol{F} \cdot \boldsymbol{X}(k-1) + \boldsymbol{\Omega} \cdot \boldsymbol{U}(k-1) + \boldsymbol{W}(k-1) \tag{24}$$

where $\boldsymbol{X}(k)$ is the PDR position vector at time k and consists of 2-dimensional position (x_k, y_k) and the step length l_k; $\boldsymbol{X}(k-1)$ is the PDR position vector at time $k-1$; $\boldsymbol{U}(k-1)$ is Wi-Fi position vector at time $k-1$, where $\boldsymbol{U}(k-1) = [x_{k-1}^{wifi}, y_{k-1}^{wifi}, 0]^T$; $\boldsymbol{F}$ is the state transition matrix; $\boldsymbol{\Omega}$ is the control matrix; $\boldsymbol{W}$ is the system noise matrix, respectively.

Algorithm 1 Adaptive Wi-Fi FTM Positioning Algorithm

Input: compensated ranging data $\boldsymbol{R}$, APs' coordinates $\boldsymbol{CD}$
Initialization: intersection result $ins \leftarrow [\,]$, $isRun \leftarrow$ true, center distance $cd \leftarrow 0$, current position $result \leftarrow [\,]$
while ($isRun$) **do**
  a. Intersection detection and radius adjustment
  for each ranging data $\boldsymbol{R}(i)$, $i \in 1, 2, \ldots, length(\boldsymbol{R})$
    if $i <$ length ($\boldsymbol{R}$) **then**
      calculate the cd of the $i-th$ and $(i+1)-th$ APs
      if $cd < [\boldsymbol{R}(i)+\boldsymbol{R}(i+1)]$ and $cd > abs[\boldsymbol{R}(i)-\boldsymbol{R}(i+1)]$ **then**
        set detection result as 1, $ins[i] \leftarrow 1$
      else do
        radius adjustment $\boldsymbol{R}(i) \leftarrow \boldsymbol{R}(i) + 1/\boldsymbol{R}(i)$
      end
    elseif i equals to the length ($\boldsymbol{R}$) **then**
      calculate the cd of the $i-th$ and the first APs
      if $cd < [\boldsymbol{R}(i)+\boldsymbol{R}(1)]$ and $cd > abs[\boldsymbol{R}(i)-\boldsymbol{R}(1)]$ **then**
        set detection result as 1, $ins[i] \leftarrow 1$
      else do
        radius adjustment $\boldsymbol{R}(i) \leftarrow \boldsymbol{R}(i) + 1/\boldsymbol{R}(i)$
      end
    end
  end
  b. position calculation using the WLS method
  if length (ins) equals the length ($\boldsymbol{R}$) **then**
    calculate the matrices $\boldsymbol{B}$, $\boldsymbol{P}$, and $\boldsymbol{L}$
    current position $result \leftarrow (\boldsymbol{B}^T\boldsymbol{P}\boldsymbol{B})^{-1}\boldsymbol{B}^T\boldsymbol{P}\boldsymbol{L}$
    $isRun \leftarrow$ false
  end
end
Output: current position $result$

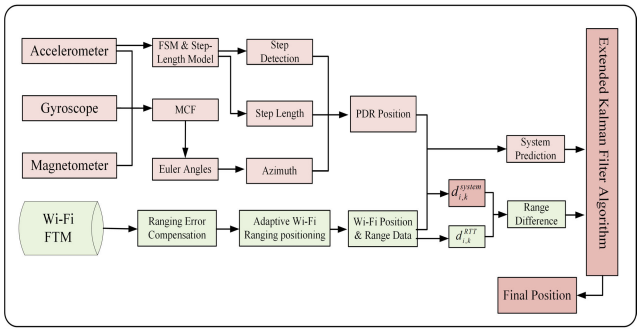

FIGURE 8. Framework of the proposed fusion positioning.

F and $\boldsymbol{\Omega}$ could be written as follows:

$$\boldsymbol{F} = \begin{bmatrix} \delta^2 & 0 & -\delta^2 sin(\psi_k) \\ 0 & \delta^2 & \delta^2 cos(\psi_k) \\ 0 & 0 & 1 \end{bmatrix} \tag{25}$$

$$\boldsymbol{\Omega} = \begin{bmatrix} \sigma^2 & 0 & 0 \\ 0 & \sigma^2 & 0 \\ 0 & 0 & \sigma^2 \end{bmatrix} \tag{26}$$

where δ^2 and σ^2 are the scale factors, and both of them are 0.5 in our research, ψ_k is the heading angle at time k.

In terms of the system observation, assuming that the planar distance between $\boldsymbol{X}(k)$ and the responder at time k is $d_{i,k}^{system}$, it can be calculated as follows:

$$d_{i,k}^{system} = \sqrt{(x_k - x_i^{RTT})^2 + (y_k - y_i^{RTT})^2} \tag{27}$$

where x_i^{RTT} and y_i^{RTT} are the coordinate values of the $i-th$ Wi-Fi FTM responder. The planar distance between the mobile phone and the responder can be defined as follows:

$$d_{i,k}^{RTT} = \sqrt{d_{i,k}^2 - (h_0 - z_i^{RTT})^2} = d_{i,k}^0 + \xi \tag{28}$$

where $d_{i,k}$ and $d_{i,k}^0$ are the measured ranging data and the theoretical planar distance between the mobile phone and the responder, respectively; ξ is the random error; h_0 and z_i^{RTT} are the heights of the carrier and the $i-th$ responder, respectively. After defining these two distances, the system observation $Z_i(k)$ can be calculated by using the difference of $d_{i,k}^{system}$ and $d_{i,k}^{RTT}$, it is expressed as follows:

$$Z_i(k) = \Delta d_i = d_{i,k}^{system} - d_{i,k}^{RTT} \tag{29}$$

If there are n responders detected, the system observation matrix $\boldsymbol{Z}(k)$ is expressed as follows:

$$\boldsymbol{Z}(k) = \left[Z_1(k)\ Z_2(k) \cdots Z_n(k) \right]^T \tag{30}$$

2) THEORETICAL VERIFICATION

In the previous section, we defined the system state and observation. However, the reason why we could build a connection between them should be clear. The following gives the verification process. First, (27) is nonlinear and it should be linearized. On the 2-dimensional plane, if there is a point $\boldsymbol{S}(k) = (x'_k, y'_k)$ that is near the $\boldsymbol{X}(k)$, we can expand (27) at $\boldsymbol{S}(k)$ by using the first-order Taylor expansion method and the linearized equation is follows:

$$Z_i(k) = d_{i,k}^0 + \left.\frac{\partial d_{i,k}^{system}}{\partial \boldsymbol{S}(k)}\right|_{\boldsymbol{X}=\boldsymbol{S}(k)} d\boldsymbol{X} + \varepsilon d\boldsymbol{X} \tag{31}$$

where $d_{i,k}^0$ is the theoretical planar distance. Combining (28) and (29), the system observation $Z_i(k)$ can be defined as follows:

$$Z_i(k) = d_{i,k}^0 + \left.\frac{\partial d_{i,k}^{system}}{\partial \boldsymbol{S}(k)}\right|_{\boldsymbol{X}=\boldsymbol{S}(k)} d\boldsymbol{X} + \varepsilon d\boldsymbol{X} - d_{i,k}^0 - \xi + v_i(k)$$

$$= \left.\frac{\partial d_{i,k}^{system}}{\partial \boldsymbol{S}(k)}\right|_{\boldsymbol{X}=\boldsymbol{S}(k)} d\boldsymbol{X} + \varepsilon d\boldsymbol{X} - \xi + v_i(k) \tag{32}$$

where ζ and $v_i(k)$ are the random errors. $\frac{\partial d_{i,k}^{system}}{\partial \boldsymbol{S}(k)}$ is the direction cosine, which is defined as follows:

$$\frac{\partial d_{i,k}^{system}}{\partial \boldsymbol{S}(k)} = \left[\frac{-(x_i^{RTT} - x'_k)}{d_{i,k}^S} \quad \frac{-(y_i^{RTT} - y'_k)}{d_{i,k}^S} \right] \tag{33}$$

where $d_{i,k}^S$ is the distance between the responder and $\boldsymbol{S}(k)$. Since $d\boldsymbol{X} = \Delta\boldsymbol{X} = [x_k - x'_k, y_k - y'_k]^T$, by taking the

third element of $\boldsymbol{X}(k)$ into account, $Z_i(k)$ can be expressed as follows:

$$Z_i(k)=\begin{bmatrix} \frac{-(x_i^{RTT}-x_k')}{d_{i,k}^S} & \frac{-(y_i^{RTT}-y_k')}{d_{i,k}^S} & 0 \end{bmatrix}\begin{bmatrix} x_k+(-x_k') \\ y_k+(-y_k') \\ l_k+(-0) \end{bmatrix} +\boldsymbol{V}_i(k) \quad (34)$$

The matrix form of (34) is as follows:

$$Z_i(k) = \boldsymbol{H}_i\cdot\boldsymbol{X}(k)+\boldsymbol{M}_i\cdot\boldsymbol{S}(k)+\boldsymbol{V}_i(k) \quad (35)$$

where $\boldsymbol{V}_i(k)$ is the measurement noise, $\boldsymbol{S}(k)$ is the position vector, where $\boldsymbol{S}(k) = [x_k', y_k', 0]^T$, and $\boldsymbol{M}_i = -\boldsymbol{H}_i$, respectively. If there are n responders detected, the system observation equation can be written as follows:

$$\boldsymbol{Z}(k)=\begin{bmatrix} Z_1(k) \\ Z_2(k) \\ \vdots \\ Z_n(k) \end{bmatrix}=\begin{bmatrix} \boldsymbol{H}_1\cdot\boldsymbol{X}(k)+\boldsymbol{M}_1\cdot\boldsymbol{S}(k)+\boldsymbol{V}_1(k) \\ \boldsymbol{H}_2\cdot\boldsymbol{X}(k)+\boldsymbol{M}_2\cdot\boldsymbol{S}(k)+\boldsymbol{V}_2(k) \\ \vdots \\ \boldsymbol{H}_n\cdot\boldsymbol{X}(k)+\boldsymbol{M}_n\cdot\boldsymbol{S}(k)+\boldsymbol{V}_n(k) \end{bmatrix} \quad (36)$$

After this step, the relationship between the system state and observation measurement has been established. The matrix representation of (36) is as follows:

$$\boldsymbol{Z}(k)=\boldsymbol{H}\cdot\boldsymbol{X}(k)+\boldsymbol{M}\cdot\boldsymbol{S}(k)+\boldsymbol{V}(k) \quad (37)$$

where $\boldsymbol{H}$ is the measurement matrix, $\boldsymbol{V}(k)$ is the measurement noise matrix, and $\boldsymbol{M}=-\boldsymbol{H}$. According to (33) and (34), the matrix $\boldsymbol{H}$ can be expressed as follows:

$$\boldsymbol{H}=\begin{bmatrix} \boldsymbol{H}_1 \\ \vdots \\ \boldsymbol{H}_n \end{bmatrix}=\begin{bmatrix} \frac{x_1^{RTT}-x_k'}{d_{1,k}^S} & \frac{y_1^{RTT}-y_k'}{d_{1,k}^S} & 0 \\ \vdots & \vdots & \vdots \\ \frac{x_n^{RTT}-x_k'}{d_{n,k}^S} & \frac{x_n^{RTT}-y_k'}{d_{n,k}^S} & 0 \end{bmatrix} \quad (38)$$

where $d_{i,k}^S$ is the distance between the $\boldsymbol{S}(k)$ and the coordinate values of $i-th$ responder, and n is the number of detected responders that have no NLOS errors. It should be noted that $\boldsymbol{S}(k)$ is near $\boldsymbol{X}(k)$. Therefore, $\boldsymbol{S}(k)$ can be calculated by using $\boldsymbol{X}(k)$ to subtract small values and setting its third element to zero. To summarize, the tightly coupled positioning system model is defined as follows:

$$\begin{cases} \boldsymbol{X}(k)=\boldsymbol{F}\cdot\boldsymbol{X}(k-1)+\boldsymbol{\Omega}\cdot\boldsymbol{U}(k-1)+\boldsymbol{W}(k-1) \\ \boldsymbol{Z}(k)=\boldsymbol{H}\cdot\boldsymbol{X}(k)+\boldsymbol{M}\cdot\boldsymbol{S}(k)+\boldsymbol{V}(k) \end{cases} \quad (39)$$

According to (39), the PDR/Wi-Fi FTM tightly coupled fusion positioning based on the EKF can be divided into six steps:

(1) System state prediction, where $k = 1, 2, 3, \ldots$:

$$\boldsymbol{X}(k+1)^- = \boldsymbol{F}\cdot\boldsymbol{X}(k)+\boldsymbol{\Omega}\cdot\boldsymbol{U}(k)+\boldsymbol{W}(k) \quad (40)$$

(2) System variance matrix prediction:

$$\boldsymbol{P}(k+1)^- = \boldsymbol{F}\cdot\boldsymbol{P}(k)\cdot\boldsymbol{F}^T+\boldsymbol{Q}_k \quad (41)$$

where $\boldsymbol{Q}_k$ is the variance of the system noise $\boldsymbol{W}(k)$.

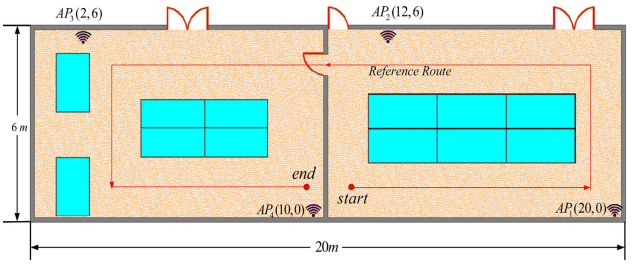

FIGURE 9. Experimental area.

(3) System observation estimation:

$$\boldsymbol{Z}(k+1)=\boldsymbol{H}\cdot\boldsymbol{X}(k+1)^-+\boldsymbol{M}\cdot\boldsymbol{S}(k+1)+\boldsymbol{V}(k+1) \quad (42)$$

(4) Calculate the kalman gain:

$$\boldsymbol{K}(k+1)=\boldsymbol{P}(k+1)\cdot\boldsymbol{H}^T\cdot[\boldsymbol{H}\cdot\boldsymbol{P}(k+1)^-\cdot\boldsymbol{H}^T+\boldsymbol{T}_k]^{-1} \quad (43)$$

where $\boldsymbol{T}_k$ is the variance of the measurement noise $\boldsymbol{V}(k)$.

(5) System state update:

$$\boldsymbol{X}(k+1)=\boldsymbol{X}(k+1)^-+\boldsymbol{K}(k+1)\cdot\left[\boldsymbol{Z}(k+1)-\boldsymbol{H}\cdot\boldsymbol{X}(k+1)^-\right] \quad (44)$$

(6) Variance matrix update:

$$\boldsymbol{P}(k+1)=(\boldsymbol{I}-\boldsymbol{K}(k+1)\cdot\boldsymbol{H})\cdot\boldsymbol{P}(k+1)^- \quad (45)$$

When the fusion positioning system runs, these six steps will be cyclically executed. Every time the state updates, the PDR position will be corrected in time by the fusion position.

IV. EXPERIMENTAL RESULTS

A. EXPERIMENTAL SETUP

As shown in Fig.9, the test area is a typical office room that contains electronic facilities and ferrous materials. Four responders with the hardware part of Intel Dual Band Wireless-AC8260 are placed at a height of 1.5 m. The sampling rates of the Wi-Fi ranging and built-in sensors are 5HZ and 25HZ, respectively. A Wi-Fi fingerprint database was constructed by setting the reference points per 1 meter, which is used to test and compare Wi-Fi fingerprint-based positioning. The red reference route was selected for fusion positioning. Four testers utilized a Google Pixel 3 mobile phone to collect data, and all the data were using the MATLAB 2016a software. It should be noted that there are high-power radars near the test rooms and they could sometimes affect the stability of magnetic field, but this phenomenon does not frequently occur.

B. ANALYSIS OF THE COMPENSATED RANGE DATA

Based on the range data collected in different environments described in part B of Section III, we set the highest order of (15) as 2 to fit these ranging errors data. As shown in Fig.10, the fitting coefficients are $a_0 = -0.058, a_1 = -0.1334$ and $a_2 = -0.0012$. Then, we apply these coefficients to the ranging error compensation model and collect

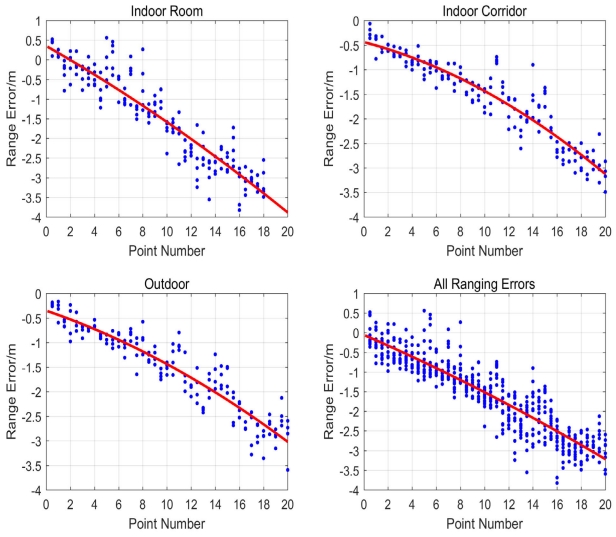

FIGURE 10. Fitting results of the ranging errors.

TABLE 2. Ranging errors comparison/(m).

Error	Min	Max	Mean	80%Error
Compensated	0.13	2.05	0.44	0.67
Uncompensated	0.45	3.83	1.56	2.60

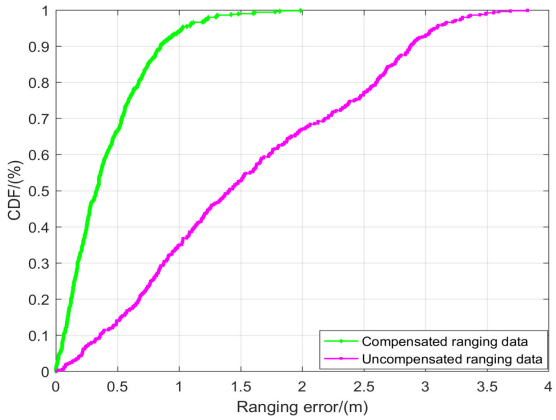

FIGURE 11. Cumulative distribution of the ranging errors.

other distance data to compare with the expected ranges. Table 2 shows that the mean ranging error and 80% errors of the compensated data are 0.41 m and 0.67 m respectively, which are better than the uncompensated ranging data. Fig.11 provides the cumulative distribution function (CDF) of the ranging errors. Our ranging model has a ranging accuracy better than 1 meter in 90% of the cases, which is better than the uncompensated ranging data.

C. ADAPTIVE WIFI FTM POSITIONING EXPERIMENT

In this section, the performance of the proposed adaptive Wi-Fi FTM positioning (AWFP) algorithm is evaluated by comparing it with the traditional Wi-Fi FTM positioning (TWFP) method using the trilateration algorithm and the

TABLE 3. Positioning errors comparison/(m).

Error	Min	Max	Mean	RMSE	80%Error
AWFP	0.19	8.60	1.96	2.93	2.57
TWFP	0.58	13.2	3.48	4.54	4.89
Fingerprint -based	0.90	10.3	3.96	4.46	5.38

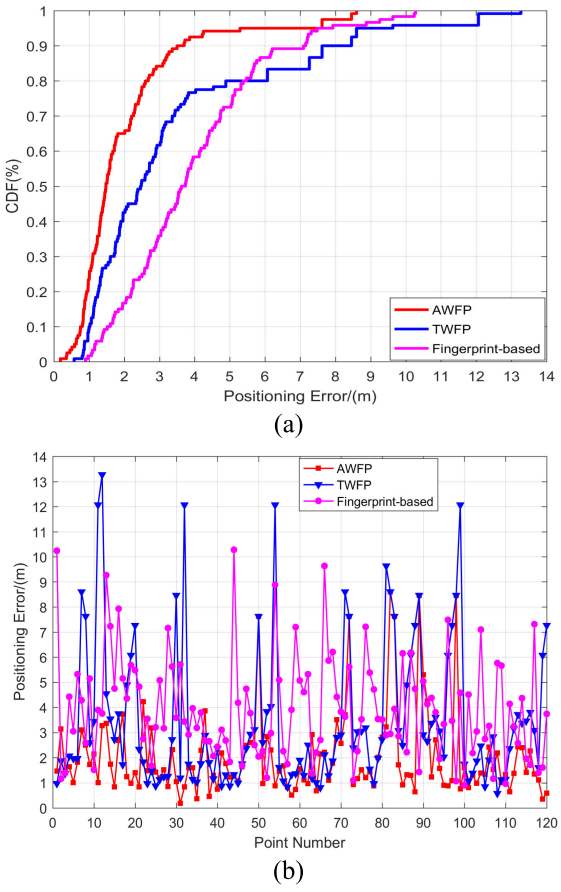

FIGURE 12. (a) Cumulative distribution of the positioning errors; and (b) Points positioning error curves.

Wi-Fi fingerprint-based location implemented based on the K-nearest neighbours algorithm (KNN) introduced in [4]. The value of K is 3. The estimated coordinates of the 120 test points are compared with their actual coordinate values. The positioning errors, CDFs, and point positioning errors are shown in Table 3 and Fig.12.

As shown in Table 3, the mean positioning accuracy and the root-mean-square error (RMSE) of AWFP are 1.96 m and 2.93 m, respectively. Compared with the TWFP and fingerprint-based method, the positioning accuracy is reduced by 1.52 m and 2.0 m, and the RMSE decreases by 1.61 m and 1.53 m, respectively. Moreover, 80% test points of AWFP have a positioning error within 2.57 m, which decreases by 2.32 m and 2.81 m compared with the other two methods. Fig.10(a) shows the cumulative distribution function (CDF) of the positioning errors and it indicates that

TABLE 4. Positioning errors of different methods/(m).

First experimenter				
Error	Min	Max	Mean	RMSE
PDR	0.16	3.80	2.26	2.56
Loosely coupled	0.17	3.05	1.42	1.61
Wi-Fi FTM	0.09	8.06	1.86	2.59
Tightly coupled	0.30	2.02	1.08	1.17
Second experimenter				
Error	Min	Max	Mean	RMSE
PDR	0.11	3.62	2.36	2.70
Loosely coupled	0.23	3.89	1.53	1.74
Wi-Fi FTM	0.12	13.3	2.21	3.14
Tightly coupled	0.12	2.38	0.90	1.13
Third experimenter				
Error	Min	Max	Mean	RMSE
PDR	0.15	4.22	2.79	3.11
Loosely coupled	0.16	4.13	1.38	1.64
Wi-Fi FTM	0.15	8.46	1.95	2.65
Tightly coupled	0.38	1.70	0.96	1.03
Fourth experimenter				
Error	Min	Max	Mean	RMSE
PDR	0.17	3.37	2.11	2.40
Loosely coupled	0.20	4.13	1.46	1.73
Wi-Fi FTM	0.21	6.46	2.01	2.56
Tightly coupled	0.18	1.76	0.97	1.05
Average results				
Error	Min	Max	Mean	RMSE
PDR	0.15	3.75	2.38	2.69
Loosely coupled	0.19	3.80	1.45	1.68
Wi-Fi FTM	0.14	9.07	2.00	2.74
Tightly coupled	0.18	1.96	0.98	1.10

AWFP has higher confidence level in different error ranges. Fig.12(b) illustrates that the points with large positioning errors of AWFP are less than the other two methods. From these error analyses, we can conclude that AWFP has better positioning performance.

D. FUSION POSITIONING EXPERIMENT

The fusion positioning experiments were conducted in the office rooms and four experimenters participated in the test. The positioning errors of different methods are shown in Table 4.

The implemented experimental results from the different testers show that the mean positioning errors and the root-mean-square errors of the proposed fusion positioning method are better than those of the PDR method, Wi-Fi FTM and loosely coupled method. The final average location error of the proposed method is 0.98 m and the RMSE is 1.10 m. The same conclusion can be easily found from Fig.13 and Fig.14, which directly show the average positioning error of the proposed method is better than the other three methods. Though the loosely coupled fusion positioning method can also provide high positioning accuracy, our proposed method reaches higher accuracy and its RMSE is also smaller than that of the loosely couple fusion positioning method.

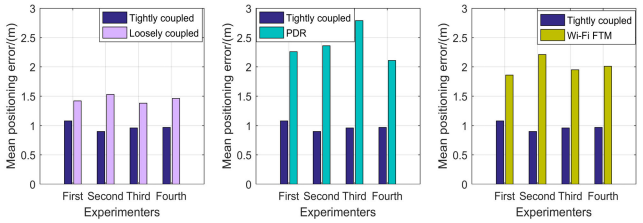

FIGURE 13. Mean positioning error comparison of different methods and experimenters.

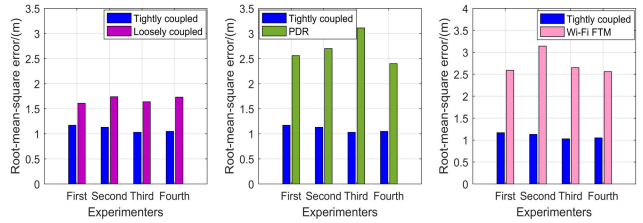

FIGURE 14. Root-mean-square error comparison of different methods and experimenters.

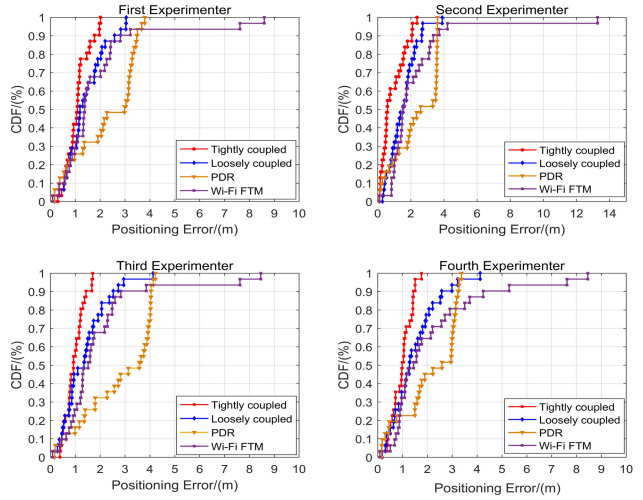

FIGURE 15. Cumulative distributions of the point positioning errors for different methods and experimenters.

To better analyse the positioning performance of our proposed fusion method, the CDF figures are illustrated in Fig.15. These figures show the same conclusion that the proposed fusion positioning method has a higher confidence level in different error ranges than the other three methods. Fig.16 shows that the trajectories of the proposed method have fewer fluctuations and are closer to the reference route. Although the loosely coupled method has a positioning accuracy of less than 2 m, its trajectories are unstable. This is because there are outliers in the Wi-Fi FTM positioning results. Since the loosely coupled method simply combines two methods' positioning results, the trajectory will generate

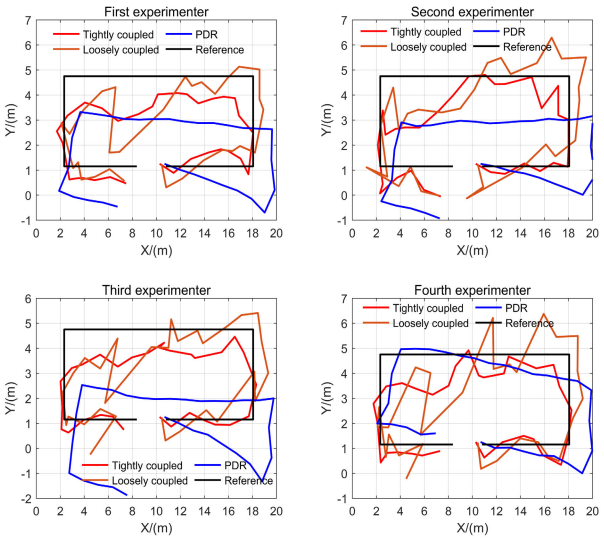

FIGURE 16. Trajectories comparison of the different methods and experimenters.

fluctuations due to the outliers. The CDF figures in Fig.15 and the stable trajectories shown in Fig.16 validate that our proposed tightly coupled method has better performance than other methods.

V. CONCLUSION

In this manuscript, we concentrated on the new Wi-Fi FTM ranging technique and studied a fusion positioning application integrating built-in mobile phone sensors. A real-time ranging error compensation model considering the NLOS error identification using the least-squares method was proposed. This ranging model could achieve a mean ranging accuracy of 0.68 m in 80% of the cases. Moreover, an adaptive Wi-Fi ranging positioning algorithm (AWFP) was devised based on high precision ranging data and the weighted least-squares algorithm. Finally, a tightly coupled fusion positioning model integrating the Wi-Fi FTM and PDR method was constructed. The experimental results showed that our proposed method had good performance regarding its mean positioning accuracy and stability compared with the PDR, Wi-Fi FTM, and the loosely coupled PDR/Wi-Fi FTM fusion positioning based on the EKF algorithm. However, some limitations also exist in our research. The azimuth of mobile phones was basically consistent with the walking direction, and the complicated pedestrian walking motions were not analysed. Moreover, the identification and elimination of NLOS errors should be studied in depth in future works.

REFERENCES

[1] P. Davidson and R. Piche, "A survey of selected indoor positioning methods for smartphones," *IEEE Commun. Surveys Tuts.*, vol. 19, no. 2, pp. 1347–1370, 2nd Quart., 2017.

[2] R. Chen and L. Chen, "Indoor positioning with smartphones: The state-of-the-art and the challenges," *Acta Geod. Cartogr. Sin.*, vol. 46, no. 10, pp. 1316–1326, Oct. 2017. doi: 10.11947/j.AGCS.2017.20170383.

[3] X. Li, X. Zhang, X. Ren, M. Fritsche, J. Wickert, and H. Schuh, "Precise positioning with current multi-constellation global navigation satellite systems: GPS, GLONASS, Galileo and BeiDou," *Sci. Rep.*, vol. 5, no. 1, p. 8328, Jul. 2015.

[4] S. He and S.-H.-G. Chan, "Wi-Fi fingerprint-based indoor positioning: Recent advances and comparisons," *IEEE Commun. Surveys Tuts.*, vol. 18, no. 1, pp. 466–490, 1st Quart., 2016.

[5] S. He, S.-H.-G. Chan, L. Yu, and N. Liu, "Fusing noisy fingerprints with distance bounds for indoor localization," in *Proc. IEEE Conf. Comput. Commun. (INFOCOM)*, Apr. 2015, pp. 2506–2514.

[6] A. Poulose, J. Kim, and D. S. Han, "A sensor fusion framework for indoor localization using smartphone sensors and Wi-Fi RSSI measurements," *Appl. Sci.*, vol. 9, no. 20, p. 4379, 2019.

[7] X. Li, J. Wang, and C. Liu, "A Bluetooth/PDR integration algorithm for an indoor positioning system," *Sensors*, vol. 15, no. 10, pp. 24862–24885, 2015.

[8] A. R. J. Ruiz, F. S. Granja, J. C. P. Honorato, and J. I. G. Rosas, "Accurate pedestrian indoor navigation by tightly coupling foot-mounted IMU and RFID measurements," *IEEE Trans. Instrum. Meas.*, vol. 61, no. 1, pp. 178–189, Jan. 2012.

[9] H. Xu, Y. Ding, P. Li, R. Wang, and Y. Li, "An RFID indoor positioning algorithm based on Bayesian probability and K-Nearest neighbor," *Sensors*, vol. 17, no. 8, p. 1806, 2017.

[10] S.-H. Fang, C.-H. Wang, T.-Y. Huang, C.-H. Yang, and Y.-S. Chen, "An enhanced ZigBee indoor positioning system with an ensemble approach," *IEEE Commun. Lett.*, vol. 16, no. 4, pp. 564–567, Apr. 2012.

[11] X. Li, Y. Wang, and K. Khoshelham, "UWB/PDR tightly coupled navigation with robust extended Kalman filter for NLOS environments," *Mobile Inf. Syst.*, vol. 2018, pp. 1–14, Dec. 2018.

[12] K. P. Subbu, B. Gozick, and R. Dantu, "LocateMe: Magnetic-fields-based indoor localization using smartphones," *ACM Trans. Intell. Syst. Technol. (TIST)*, vol. 4, no. 4, pp. 1–27, Sep. 2013.

[13] S. He and K. G. Shin, "Crowd-flow graph construction and identification with spatio-temporal signal feature fusion," in *Proc. IEEE INFOCOM-IEEE Conf. Comput. Commun.*, Apr. 2019, pp. 757–765.

[14] S. He and K. G. Shin, "Geomagnetism for smartphone-based indoor localization: Challenges, advances, and comparisons," *ACM Comput. Surv.*, vol. 50, no. 6, pp. 1–37, Dec. 2017.

[15] L. Zheng, W. Zhou, W. Tang, X. Zheng, A. Peng, and H. Zheng, "A 3D indoor positioning system based on low-cost MEMS sensors," *Simul. Model. Pract. Theory*, vol. 65, pp. 45–56, Jun. 2016.

[16] A. Poulose, O. S. Eyobu, and D. S. Han, "An indoor position-estimation algorithm using smartphone IMU sensor data," *IEEE Access*, vol. 7, pp. 11165–11177, 2019.

[17] J. Kuang, X. Niu, and X. Chen, "Robust pedestrian dead reckoning based on MEMS-IMU for smartphones," *Sensors*, vol. 18, no. 5, p. 1391, 2018.

[18] T. Sun, L. Zheng, A. Peng, B. Tang, and G. Ou, "Building information aided Wi-Fi fingerprinting positioning system," *Comput. Electr. Eng.*, vol. 71, pp. 558–568, Oct. 2018.

[19] S. A. Golden and S. S. Bateman, "Sensor measurements for Wi-Fi location with emphasis on time-of-arrival ranging," *IEEE Trans. Mobile Comput.*, vol. 6, no. 10, pp. 1185–1198, Oct. 2007.

[20] X. Li, K. Pahlavan, M. Latva-aho, and M. Ylianttila, "Comparison of indoor geolocation methods in DSSS and OFDM wireless LAN systems," in *Proc. Veh. Technol. Conf. Fall . IEEE VTS Fall VTC. 52nd Veh. Technol. Conf.*, vol. 6, Sep. 2000, pp. 3015–3020.

[21] Z. Yang, Z. Zhou, and Y. Liu, "From RSSI to CSI: Indoor localization via channel response," *ACM Comput. Surv.*, vol. 46, no. 2, pp. 25:1–25:32, Nov. 2013.

[22] J. Zhou, L. Shen, and Z. Sun, "A new method of D-TDOA time measurement based on RTT," *MATEC Web Conf.*, vol. 207, Sep. 2018, Art. no. 03018.

[23] L. Banin, U. Schatzberg, and Y. Amizur, "Next generation indoor positioning system based on WiFi time of flight," in *Proc. 26th Int. Tech. Meeting Satell. Division Inst. Navigat.(ION GNSS+)*, Sep. 2013, pp. 975–982.

[24] *IEEE Standard for Information Technology-Telecommunications and Information Exchange Between Systems Local and Metropolitan Area Networks-Specific Requirements—Part 11: Wireless LAN Medium Access Control (MAC) and Physical Layer (PHY) Specifications*, IEEE Standard 802.11-2016 and 802.11-2012, Dec. 2016.

[25] Z. Liu, L. Zhang, Q. Liu, Y. Yin, L. Cheng, and R. Zimmermann, "Fusion of magnetic and visual sensors for indoor localization: Infrastructure-free and more effective," *IEEE Trans. Multimedia*, vol. 19, no. 4, pp. 874–888, Apr. 2017.
[26] Y. Li, Y. Zhuang, P. Zhang, H. Lan, X. Niu, and N. El-Sheimy, "An improved inertial/WiFi/magnetic fusion structure for indoor navigation," *Inf. Fusion*, vol. 34, pp. 101–119, Mar. 2017.
[27] H. Hellmers, A. Norrdine, J. Blankenbach, and A. Eichhorn, "An IMU/magnetometer-based indoor positioning system using Kalman filtering," in *Proc. Int. Conf. Indoor Positioning Indoor Navigat.*, Montbeliard-Belfort, France, Oct. 2013, pp. 1–9.
[28] A. G. Ferreira, D. Fernandes, A. P. Catarino, A. M. Rocha, and J. L. Monteiro, "A loose-coupled fusion of inertial and UWB assisted by a decision-making algorithm for localization of emergency responders," *Electronics*, vol. 8, no. 12, p. 1463, Dec. 2019.
[29] Y.-S. Cho, M.-I. Ji, J.-Y. Kim, and J.-I. Jeon, "High-scalable 3D indoor positioning algorithm using loosely-coupled Wi-Fi/sensor integration," in *Proc. 17th Int. Conf. Adv. Commun. Technol. (ICACT)*, Seoul, South Korea, July. 2015, pp. 96–99.
[30] V. Radu and M. K. Marina, "HiMLoc: Indoor smartphone localization via activity aware pedestrian dead reckoning with selective crowdsourced WiFi fingerprinting," in *Proc. Int. Conf. Indoor Positioning Indoor Navigat.*, Montbeliard-Belfort, France, Oct. 2013, pp. 1–10.
[31] D. D. McCrady, L. Doyle, H. Forstrom, T. Dempsey, and M. Martorana, "Mobile ranging using low-accuracy clocks," *IEEE Trans. Microw. Theory Techn.*, vol. 48, no. 6, pp. 951–958, Jun. 2000.
[32] L. Banin, U. Schatzberg, and Y. Amizur, "WiFi FTM and map information fusion for accurate positioning," in *Proc. Int. Conf. Indoor Position. Indoor Navigat. (IPIN)*, 2016, pp. 1–4.
[33] N. Dvorecki, O. Bar-Shalom, L. Banin, and Y. Amizur, "A machine learning approach for Wi-Fi RTT ranging," in *Proc. Int. Tech. Meeting Inst. Navigat.*, Reston, VA, USA, Feb. 2019, pp. 435–444.
[34] P. J. Voltz and D. Hernandez, "Maximum likelihood time of arrival estimation for real-time physical location tracking of 802.11a/g mobile stations in indoor environments," in *Proc. Position Location Navigat. Symp. (PLANS)*, Apr. 2004, pp. 585–591.
[35] M. Ibrahim, H. Liu, M. Jawahar, V. Nguyen, M. Gruteser, R. Howard, F. Bai, and B. Yi, "Verification: Accuracy evaluation of WiFi fine time measurements on an open platform," in *Proc. 24th Annu. Int. Conf. Mobile Comput. Netw.*, 2018, pp. 417–427.
[36] *Wi-Fi Location: Ranging With RTT| Android Developers*. Accessed: 2019. [Online]. Available: https://developer.android.com/guide/topics/connectivity/wifi-rtt.html
[37] Y. Yu, R. Chen, L. Chen, G. Guo, F. Ye, and Z. Liu, "A robust dead reckoning algorithm based on Wi-Fi FTM and multiple sensors," *Remote Sens.*, vol. 11, no. 5, p. 504, 2019.
[38] S. Xu, R. Chen, Y. Yu, G. Guo, and L. Huang, "Locating smartphones indoors using built-in sensors and Wi-Fi ranging with an enhanced particle filter," *IEEE Access*, vol. 7, pp. 95140–95153, 2019.
[39] L. Banin, O. Bar-Shalom, N. Dvorecki, and Y. Amizur, "Scalable Wi-Fi client self-positioning using cooperative FTM-sensors," *IEEE Trans. Instrum. Meas.*, vol. 68, no. 10, pp. 3686–3698, Oct. 2019.
[40] V. Renaudin, C. Combettes, and F. Peyret, "Quaternion based heading estimation with handheld MEMS in indoor environments," in *Proc. IEEE/ION Position, Location Navigat. Symp. (PLANS)*, Monterey, CA, USA, May 2014, pp. 645–656.
[41] J. Liu, R. Chen, L. Pei, R. Guinness, and H. Kuusniemi, "A hybrid smartphone indoor positioning solution for mobile LBS," *Sensors*, vol. 12, no. 12, pp. 17208–17233, 2012.
[42] A. Poulose, J. Kim, and D. S. Han, "Indoor localization with smartphones: Magnetometer calibration," in *Proc. IEEE Int. Conf. Consum. Electron. (ICCE)*, Las Vegas, NV, USA, Jan. 2019, pp. 1–3.
[43] A. Poulose, B. Senouci, and D. S. Han, "Performance analysis of sensor fusion techniques for heading estimation using smartphone sensors," *IEEE Sensors J.*, vol. 19, no. 24, pp. 12369–12380, Dec. 2019.
[44] R. Mahony, T. Hamel, and J.-M. Pflimlin, "Nonlinear complementary filters on the special orthogonal group," *IEEE Trans. Autom. Control*, vol. 53, no. 5, pp. 1203–1218, Jun. 2008.
[45] E. Buckwar and M. G. Riedler, "Runge–Kutta methods for jump–diffusion differential equations," *J. Comput. Appl. Math.*, vol. 236, no. 6, pp. 1155–1182, Oct. 2011.
[46] D. Ahn, J.-S. Park, C.-S. Kim, J. Kim, Y. Qian, and T. Itoh, "A design of the low-pass filter using the novel microstrip defected ground structure," *IEEE Trans. Microw. Theory Techn.*, vol. 49, no. 1, pp. 86–93, Jan. 2001.
[47] L. Keselbrener, M. Keselbrener, and S. Akselrod, "Nonlinear high pass filter for R-wave detection in ECG signal," *Med. Eng. Phys.*, vol. 19, no. 5, pp. 481–484, Jun. 1997.
[48] P. Zhang and F. Li, "A new adaptive weighted mean filter for removing salt-and-pepper noise," *IEEE Signal Process. Lett.*, vol. 21, no. 10, pp. 1280–1283, Oct. 2014.
[49] A. Brajdic and R. Harle, "Walk detection and step counting on unconstrained smartphones," in *Proc. ACM Int. Joint Conf. Pervas. Ubiquitous Comput. (UbiComp)*, 2013, pp. 225–234.
[50] Y. Zhuang, H. Lan, Y. Li, and N. El-Sheimy, "PDR/INS/WiFi integration based on handheld devices for indoor pedestrian navigation," *Micromachines*, vol. 6, no. 6, pp. 793–812, 2015.
[51] Q. Ladetto, "On foot navigation: Continuous step calibration using both complementary recursive prediction and adaptive Kalman filtering," in *Proc. ION GPS*, Salt Lake City, UT, USA, 2000, pp. 1735–1740.
[52] E. Vildjiounaite, E.-J. Malm, J. Kaartinen, and P. Alahuhta, "Location estimation indoors by means of small computing power devices, accelerometers, magnetic sensors, and map knowledge," in *Pervasive Computing* (Lecture Notes in Computer Science), vol. 2414. Berlin, Germany: Springer, Jan. 2002, pp. 211–224.
[53] Q. Tian, Z. Salcic, K. I.-K. Wang, and Y. Pan, "A multi-mode dead reckoning system for pedestrian tracking using smartphones," *IEEE Sensors J.*, vol. 16, no. 7, pp. 2079–2093, Apr. 2016.
[54] H. Weinberg, "Using the ADXL202 in pedometer and personal navigation applications," Analog Devices Appl. Notes AN-602, 2002, pp. 1–6, vol. 2.
[55] A. Poulose, O. S. Eyobu, and D. S. Han, "A combined PDR and Wi-Fi trilateration algorithm for indoor localization," in *Proc. Int. Conf. Artif. Intell. Inf. Commun. (ICAIIC)*, Okinawa, Japan, Feb. 2019, pp. 72–77.

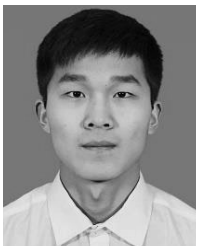

MENG SUN received the bachelor's degree in surveying and mapping engineering from the China University of Mining and Technology (CUMT), Xuzhou, China, in 2018, where he is currently pursuing the Ph.D. degree in geodesy and survey engineering. He was an Assistant with Undergraduate Teaching Office, in 2017. His research interests include indoor positioning and navigation, and indoor and outdoor detection.

YUNJIA WANG is currently a Professor and the Director of the Key Laboratory of Land Environment and Disaster Monitoring, MNR, CUMT. He was the President with the School of Environment Science and Spatial Informatics, CUMT, China, from 2007 to 2016. He is currently a Committee Member of the International Society of Mine Surveying, China National Bureau of Surveying and Mapping Geographic. He has published more than 200 manuscripts. His current research interests include indoor and outdoor seamless positioning, In-SAR, assessment and management of resources and environment, and geographic information engineering. He is also the Editorial Member of the *Journal of Resources and Ecology*, *Acta Geodaetica et Cartographica Sinica*, and *Bulletin of Surveying and Mapping*.

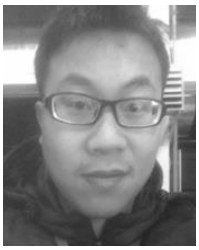

SHENGLEI XU received the bachelor's degree in surveying engineering from the China University of Mining and Technology (CUMT), Xuzhou, China, in 2014, where he is currently pursuing the Ph.D. degree in the geodesy and survey engineering. From 2014 to 2018, he studied geodesy and survey engineering at CUMT. His research interests include indoor positioning and navigation.

HONGXIA QI received the bachelor's degree in information management from the North China University of Science and Technology, Hebei, China, in 2008, and the master's degree from Beijing Jiaotong University, Beijing, China, in 2010. She is currently pursuing the Ph.D. degree in cartography and geographic information engineering with the China University of Mining and Technology (CUMT), Xuzhou, China. Her research interest includes indoor positioning and navigation.

XIANXIAN HU received the bachelor's degree in surveying engineering from the China University of Mining and Technology (CUMT), Xuzhou, China, in 2018, where he is currently pursuing the master's degree in the geodesy and survey engineering. His research interest includes indoor and outdoor seamless positioning.